

## A Comparative Study of the Sintering and Cell Behavior of Pure and Cobalt-Substituted Hydroxyapatite

Erica Kramer<sup>1</sup>, Matthew Conklin<sup>2</sup>, Michael Zilm<sup>1</sup>, Emily Itzkowitz<sup>2</sup> and Mei Wei<sup>1\*</sup>

<sup>1</sup>Department of Materials Science and Engineering, Institute of Materials Science, University of Connecticut, 97 North Eagleville Rd., Storrs, CT 06269, USA

<sup>2</sup>Biomedical Engineering Program, University of Connecticut, 260 Glenbrook Rd, Storrs, CT 06269, USA

### Abstract

Hydroxyapatite (HA) is a widely studied biomaterial for bone grafting and tissue engineering applications. The crystal structure of HA lends itself to a wide variety of substitutions, which allows for tailoring of material properties. Cobalt is of interest in ion substitution in HA due to its magnetic properties. The synthesis and characterization of cobalt-substituted Hydroxyapatite (CoHA) has not been widely studied, and there is a complete lack of studies on the sintering behaviors of CoHA materials compared to pure HA. Studying the sintering behavior of a substituted apatite provides insight into which applications are appropriate for the substituted material by supplying information regarding how the substitution affects material characteristics such as stability and bulk mechanical properties. In this study both pure HA and CoHA were synthesized, pressed into pellets, and then sintered at temperatures ranging from 900-1300°C and 700-1200°C, respectively. The study thoroughly examined the comparative sintering behaviors of the two materials. It was found that CoHA is less thermally stable than pure HA, with decomposition to TCP beginning around 1200°C for pure HA samples, while at 800°C for the CoHA. The CoHA also had a lower mechanical strength than that of the pure HA. Although the CoHA would be unsuitable for bulk applications, it is a promising material for a variety of biomedical applications including drug delivery, cancer hyperthermia, and as a MRI contrast agent.

**Keywords:** Hydroxyapatite; Ion substitution; Sintering behavior; Cell culture

### Introduction

Biomaterials are widely studied for applications related to traditional medical devices, diagnostic products, smart drug delivery systems, and tissue engineering and regenerative medicine systems. Biomaterials research takes advantage of developments in traditional materials science fields, but is also concerned with the biocompatibility and biofunctionality of candidate biomaterials [1]. The ceramic class of biomaterials has been studied in the past particularly for use in applications in bone augmentation and replacement [1,2]. Ceramic powder properties, such as crystallinity, surface area, and particle size, determine their effectiveness for specific applications. Additionally, powder properties and chemical composition affect material sinterability [3]. A study of a ceramic's sintering behavior can provide insight into material stability and bulk mechanical properties, thereby determining which applications are appropriate for the material.

One such ceramic material which has been widely studied in the field of biomaterials is hydroxyapatite (HA), due to the fact that HA is the main mineral phase of natural bone [2,4,5]. It is commonly used in bone grafting and tissue engineering applications due to its excellent biocompatibility and osteoconductivity [6]. HA,  $\text{Ca}_{10}(\text{PO}_4)_6(\text{OH})_2$ , has a hexagonal crystal lattice structure [7] that allows for a wide variety of substitutions by anions, cations, and functional groups, such as F<sup>-</sup> [8], Fe<sup>2+/3+</sup> [9-14], and CO<sub>3</sub><sup>2-</sup> [15]. These substitutions can tailor the physical, chemical, mechanical, and biological properties of HA making it suitable for broader biomedical applications.

Among the HA properties that can be modified by substitutions are magnetic properties. Pure HA is diamagnetic, but the substitution or incorporation of metal ions with magnetic properties can yield HA with magnetic properties. Potential biomedical applications for biocompatible nanoparticles with magnetic properties are widespread. Such applications include drug delivery, medical imaging,

or hyperthermia based cancer therapies [11,16-20]. Because HA is highly biocompatible and biodegradable, the application of HA with magnetic properties will minimize the toxicity and non-degradability concerns that are currently a widespread issue in these fields which currently employ iron oxides as magnetic nanoparticles for biomedical applications [21].

Currently, the most commonly applied method to yield HA with magnetic properties is the fabrication of iron-substituted apatite [9-14]. Another possible substitution that may result in magnetic properties is the substitution of cobalt ions for calcium ions in the HA crystal lattice. There have been limited studies recently on the substitution of cobalt into the HA lattice. Stojanovic et al. and Veselinovic et al. synthesized CoHA via hydrothermal treatment where Co<sup>2+</sup> substituted for Ca<sup>2+</sup> up to about 12 atomic % [22,23]. Careful analysis was conducted on the crystal structure of the resulting material, but limited results were reported regarding the effect that cobalt substitution had on other material properties. The objective of this work was to provide a systematic study of the sintering behavior and corresponding mechanical properties at a series of temperatures, to determine the appropriateness of CoHA for various types of biomedical applications.

### Materials and Methods

**\*Corresponding author:** Mei Wei, Department of Materials Science and Engineering, Institute of Materials Science, University of Connecticut, 97 North Eagleville Rd., Storrs, CT 06269, USA, Tel: (860) 486-9253; E-mail: [meiwei@engr.uconn.edu](mailto:meiwei@engr.uconn.edu)

**Received** May 15, 2014; **Accepted** September 18, 2014; **Published** September 29, 2014

**Citation:** Kramer E, Conklin M, Zilm M, Itzkowitz E, Wei M (2014) A Comparative Study of the Sintering and Cell Behavior of Pure and Cobalt-Substituted Hydroxyapatite. *Bioceram Dev Appl* 4: 077. doi: [10.4172/2090-5025.1000077](https://doi.org/10.4172/2090-5025.1000077)

**Copyright:** © 2014 Kramer E, et al. This is an open-access article distributed under the terms of the Creative Commons Attribution License, which permits unrestricted use, distribution, and reproduction in any medium, provided the original author and source are credited.

## Hydroxyapatite and cobalt-substituted hydroxyapatite synthesis

Hydroxyapatite powder was prepared via a wet precipitation procedure in which an aqueous solution of 2 g/dL ammonium phosphate (99+%, Acros) was added dropwise at a moderate dropping rate of about 75 drops per minute under vigorous stirring to a 2 g/dL aqueous calcium nitrate tetrahydrate (99%, Fisher) solution at 75°C. Ammonium hydroxide (~30%, Fisher) was also added to the phosphate solution to bring up the pH to 11-12 prior to mixing the two solutions. After 3 hours of stirring at 75°C, the HA particles were collected by filtration and washed thoroughly with deionized water. The collected HA precipitates were dried at 90°C for 12-16 hours and ground by mortar and pestle into a fine powder.

Cobalt was incorporated during HA synthesis using the synthesis procedure as described above. A quantity of cobalt (II) chloride that would allow for 10% substitution was added to the phosphate-containing solution. The rest of the synthesis was conducted exactly as described for pure HA. This resulting powders were then milled (SPEX 8000 Mixer/Mill) for 10 minutes in a steel canister with alumina milling balls.

Cobalt was also incorporated via ion exchange for use in the cell culture study. HA powder was subjected to a simple soaking procedure to achieve cobalt substitution for calcium in the HA crystal lattice. HA powder was soaked in a cobalt chloride solution at a concentration of 0.02 M under moderate stirring for one hour at room temperature, and then collected by filtration and washed by deionized water. The resulting powder was dried and ground manually, and then sterilized with 70% ethanol.

## Pellet preparation and sintering

Milled HA and CoHA powders were uniaxially pressed into pellets using a bench top laboratory press (CM, 1610FL). For each pellet, 0.35 g of powder was pressed into a 13 mm pellet die well lubricated with stearic acid (97%, Acros) in acetone (99.9%, J.T. Baker) at a pressure of 150 MPa for 10 seconds. The resultant HA pellets had a thickness of approximately 1.63 mm and the CoHA pellets had a thickness of 1.80 mm.

Pellets were sintered at a selection of temperatures for each sample type using a ramp rate of 5°C per minute and soaked at peak temperature for 2 hours in a chamber furnace (CM, 1610FL). The sintering temperatures used were 900, 1000, 1100, 1200, and 1300°C for HA samples, and 700, 800, 900, 1000, 1100 and 1200°C for CoHA samples. Lower sintering temperatures were selected for the CoHA samples after preliminary results for samples run at the same temperatures as pure HA indicated that decomposition began for CoHA at temperatures below 900°C. A total of 10 pellets of each type of powder were sintered for each temperature point investigated.

## Sample characterization

**Starting powder characterization:** The starting powder was characterized in other work [24] using energy dispersive X-ray spectroscopy (EDX) to verify the presence of cobalt in the sample powders. A Thermo Noran EDS detector coupled to a JEOL JSM 6335 field emission scanning electron microscope (FESEM) was used for chemical analysis. Powder samples of HA and CoHA were examined using a Bruker D2 Phaser X-ray diffractometer with a copper target, and voltage and current conditions of 40 kV and 40

mA, respectively. Conditions used were a 0.02° 2-theta step size and a scan speed of 4°/min with a 2-theta range of 10-90. XRD was used to analyze sample crystal structure. Additionally, a Niclotet Magna 560 Fourier Transform Infrared (FT-IR) Spectrometer was used to compare the functional groups of pure HA and the CoHA samples. This characterization was carried out using classic KBr pellet technique in a transmission mode. Each FT-IR spectrum was the average of 32 scans with a resolution of 4.0 cm<sup>-1</sup> in the range of 400-4000 cm<sup>-1</sup>. CoHA powder magnetic properties were analyzed using a Quantum Design MPMS-5 superconducting quantum interference device (SQUID) magnetometer. Powder sample magnetization measurements were carried out for magnetic fields - 50kOe < H < + 50kOe at 300 K.

**Density and biaxial flexural strength:** Density measurements were performed on green and sintered pellets using an Ohaus digital balance accurate to 1 mg and a caliper (Mitutoyo) accurate to 0.01 mm. Three diameter and three thickness measurements were taken for each of the 10 pellets sintered at each temperature and the respective averages were used when calculating pellet density. Sintered pellets were also observed for visual appearance changes. A Tinius Olsen (150KS model) was used to determine the pellet biaxial flexure strength (modulus of rupture) on 13 mm diameter pellets (n=8) using a 1000 N load cell at a crosshead speed of 0.01 mm/minute and a pin-on-disc test fixture set up per ASTM F 394 [25]. The modulus of rupture (MOR) was calculated based on the following equations:

$$S = -0.2387 P(X-Y)/d^2 \quad (1)$$

Where S = maximum center tensile stress (MPa), P = total load causing fracture (N),

$$X = (1+\nu) \ln[(B/C)^2] + [(1-\nu)/2](B/C)^2, \quad (2)$$

$$Y = (1+\nu) [1+\ln[(A/C)^2]] + (1-\nu)(A/C)^2, \quad (3)$$

Where  $\nu$  = Poisson's ratio, 0.27, A = radius of support circle (mm), B = radius of loaded area or pin tip (mm), C = radius of specimen (mm), and d = specimen thickness at point of fracture (mm).

**XRD characterization:** As-prepared HA and CoHA, and those sintered at different temperatures were examined for phase purity and crystal structure using a Bruker D2 Phaser X-ray diffractometer (XRD) with a copper target, and voltage and current conditions of 40 kV and 40 mA, respectively. Conditions used were a 0.02° 2-theta step size and a scan speed of 4°/min with a 2-theta range of 10-60.

**FESEM characterization:** Field emission scanning electron microscopy (FESEM) was used to examine the cross-section morphology of sintered pellets with an accelerating voltage of 10 kV. Fractured pellets from mechanical testing were used, and pellet cross-sections were left unpolished and sputter coated with gold palladium for 1 minute prior to imaging at 10,000x.

**Cell culture study:** The biocompatibility of CoHA was assessed through cell proliferation and damage to cell membranes. Proliferation was monitored through the reduction of a tetrazolium dye, and the integrity of the cell membrane was quantified through released lactate dehydrogenase (LDH).

Mouse calvaria 3T3-E1 cells were used for the study. Cells were grown in alpha modified eagles medium (MEM) supplemented with 10% fetal bovine serum and 1% penicillin-streptomycin at 37°C under an atmosphere of 5% CO<sub>2</sub> with changes in medium every other day until 90% confluence, at which point, cells were harvested and seeded at 10,000 cells per well in a 48 well plate for proliferation assays and

10,000 cells per well in a 96 well plate for LDH assay. A period of 24 hours were allotted for cell attachment, after which cells were treated with the supernatant of a HA or CoHA, prepared via synthesis or ion exchange, solution. In previous work [24] it was found that the surface compositions and cobalt content of CoHA generated by wet synthesis and CoHA prepared via ion exchange differed. In order to ensure that these differences did not have measurable effects on cell viability both CoHA powder types were included in this study. The HA and CoHA supernatant solutions were prepared by dispersing un-sintered particles, that were previously dispersed in 70% ethanol and rinsed three times with sterile de-ionized water, at concentrations of 20, 50 or 100  $\mu\text{g}/\text{ml}$  in alpha-MEM. Each condition was tested in quadruplicate.

For the proliferation assay the medium was changed every day and the amount of used solution was replaced with an equal volume of alpha-MEM. At day 1, 3 and 7 the proliferation was assessed by replacing the medium with fresh alpha-MEM and adding a 5 mg/ml MTT working solution equal to 1/10<sup>th</sup> the medium volume. The treated cells were incubated for 4 hours at 37°C. The medium was then removed and a solution of 0.04 N HCl in isopropanol was added to dissolve the formed crystals. Aliquots of 200  $\mu\text{l}$  were measured using a microplate reader (Biotek) at 560 nm and the background absorbance was measured at 680 nm.

LDH activity was evaluated with a LDH assay kit from Thermo Scientific. In brief, after the cell attachment period cells were treated with 100  $\mu\text{l}$  of supernatant medium from CoHA via wet synthesis or ion exchange, and for positive and negative controls one set of cells were treated with the provided lysis solution for maximum LDH release and another set of cells were treated with cell culture medium only. After incubation for 24 hours 50  $\mu\text{l}$  of working solution was added to the medium and the plate was incubated for 30 minutes at room temperature in the dark. The stop solution, 50  $\mu\text{l}$ , was then added to the medium and 150  $\mu\text{l}$  aliquots were taken for measurement. The absorbance of the aliquots was measured at 480 nm and the background was measured at 680 nm.

## Results

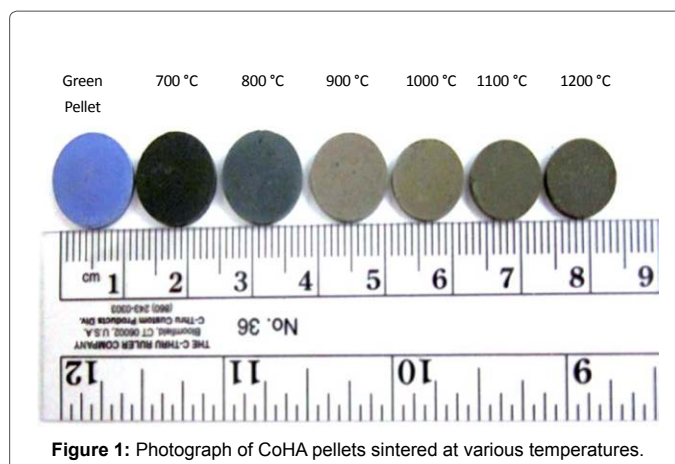
### Starting powder characterization

The CoHA powder was characterized thoroughly in previous work and the findings are briefly summarized here [24]. EDX confirmed the presence of cobalt in the CoHA sample powder. The powder was analyzed for crystal structure and phase purity using X-ray diffraction and Fourier transform infrared spectroscopy. Additionally, magnetic properties were studied using superconducting quantum interference device analysis. The results showed that after cobalt substitution the powder retained characteristic apatite crystal structure and functional groups. Additionally, cobalt substituted samples displayed paramagnetic properties, as opposed to the diamagnetism of pure HA.

### Density and biaxial flexural strength

After sintering HA and CoHA pellets were observed for visual change. The HA pellets underwent shrinkage but otherwise retained their white appearance with flat top and bottom surfaces. The CoHA pellets, on the other hand, underwent not only shrinkage but also an obvious color change upon sintering.

Figure 1 is a photograph of green and sintered CoHA pellets showing the change in color that accompanied the sintering procedure at each temperature point. Un-sintered CoHA pellets demonstrate a bright purple, but upon sintering the color changes drastically. Pellets



sintered at 700°C exhibit such a dark color that they look essentially black. Sintering at 800°C results in dark charcoal grey. Pellets sintered at temperatures from 900 to 1200°C all display grey coloring, which gets darker with increasing temperature. In addition to getting darker, the grey becomes increasingly muddy and brownish. Although the CoHA pellets undergo distinct color changes, they also retain the typical flat surfaced appearance of the HA pellets, and diameter shrinks with increasing sintering temperature.

Both green and sintered densities were measured for HA and CoHA, with 10 pellets being measured at each sintering temperature examined for each powder type. Density values were recorded as the average of these measurements. Sintered densities as a function of sintering temperature for both HA and CoHA pellets are shown in Figure 2.

The average green density for pure HA pellets was 1.65  $\text{g}/\text{cm}^3$  and the average green density of CoHA pellets was 1.42  $\text{g}/\text{cm}^3$ . The HA sintered densities increased with sintering temperature up to a maximum density of 2.92  $\text{g}/\text{cm}^3$  at 1200°C, and then dropped at 1300°C. The peak density achieved was 90% the theoretical density of HA. CoHA sintered densities increased with sintering temperature, to a maximum density of 2.46  $\text{g}/\text{cm}^3$  at 1200°C. With an increase in sintering temperature from 900°C to 1200°C the HA pellets shrank in diameter from 10.66 mm after 900°C sintering to 10.17 mm after 1200°C sintering. The average sintered diameter of the 1300°C pellets increased slightly to 10.21 mm. Sintered thickness also shrank with an increase in sintering temperature up to 1200°C, from 1.43 mm after 900°C to 1.33 mm after 1200°C sintering. Average thickness after sintering at 1300°C was 1.37 mm. There was a decrease in CoHA average sintered diameter and thickness with increase in sintering temperature from 700°C to 1200°C. The average pellet diameters shrank from 12.29 mm after 700°C to 10.09 mm after 1200°C, and pellet thickness shrank from 1.72 mm to 1.48 mm.

After pellet densities were measured, the pellets were subjected to a modulus of rupture (MOR) test to study mechanical properties of the sintered pellets. The results of the MOR test are summarized in Figure 3. The values are presented as averages plus/minus standard deviations.

The MOR of the sintered HA samples ranged from the lowest value of 29.13 MPa for pellets sintered at 1300°C to a peak value of 56.50 MPa for pellets sintered at 1000°C. Samples sintered at 900, 1100, and 1200°C had MOR values of 36.5, 54.34, and 50.41 MPa respectively (Figure 3). The MOR of the CoHA sintered samples were at a low of 10.02 MPa for the samples sintered at 700°C and a high of 28.86 MPa

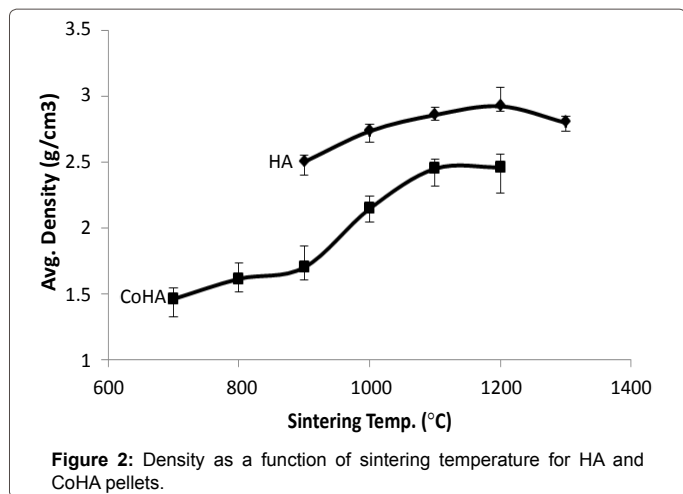


**Figure 2:** Density as a function of sintering temperature for HA and CoHA pellets.

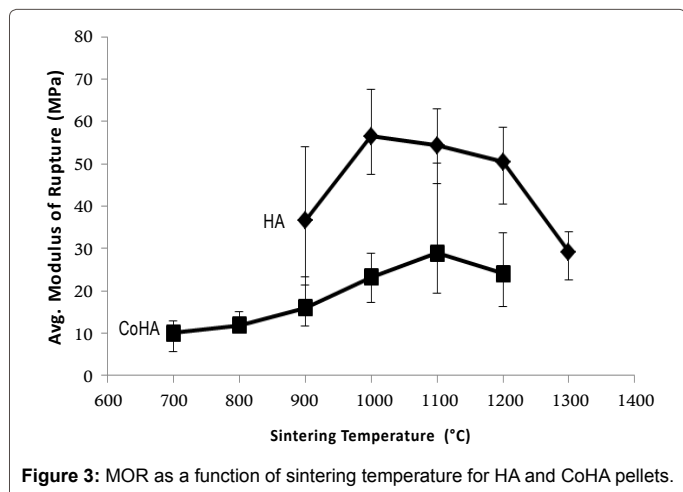


**Figure 3:** MOR as a function of sintering temperature for HA and CoHA pellets.

for the samples sintered at 1100°C. At sintering temperatures of 800, 900, 1000, and 1200°C, MOR values were 11.80, 15.89, 23.18, and 24.08 MOR, respectively.

An ANOVA analysis was conducted on the mean MOR values resulting from 6 to 8 measurements at each temperature for both HA and CoHA. This analysis resulted in a p-value of  $2.89 \times 10^{-5}$  for the HA samples, thus there is a significant difference ( $p < 0.05$ ) between the MOR values for the HA pellets sintered at different temperatures. ANOVA analysis for the CoHA samples resulted in a p-value of  $2.64 \times 10^{-7}$ , indicating significant difference between the MOR values for the CoHA pellets sintered at different temperatures.

### XRD characterization

Crystal structure and phase purity of the sintered HA and CoHA pellets were examined using XRD. The resulting XRD spectra are shown in Figure 4 for HA and Figure 5 for CoHA.

HA sintered samples resulted in XRD spectra containing peaks that are identical to those present in the un-sintered HA control spectrum and match well with the HA JCPD reference card 9-432 for temperatures up to 1200°C. At 1200°C, an extraneous peak emerges at about  $30^\circ 2\theta$  which would match with the TCP peak at  $29.68^\circ 2\theta$ .

CoHA sintered samples result in XRD spectra that do not match completely with the unsintered control sample. Extraneous peaks at

about  $13.7^\circ$ ,  $28.0^\circ$ , and  $31.3^\circ 2\theta$ , which can be matched to TCP, emerge at sintering temperatures as low as 800°C. Additionally, starting at 700°C, there is an extraneous peak that emerges at about  $36.5^\circ 2\theta$ , which can likely be assigned to a cobalt oxide phase. In both HA and CoHA sintering led to sharper XRD peaks, indicating improved crystallinity as compared to the green samples.

### FESEM characterization

Unpolished fracture surfaces of the sintered pellets were imaged using FESEM allowing the observation of the microporosity of these samples and the extent to which the samples have been sintered to be examined. Figure 6 contains the micrographs of the HA pellet cross-sections sintered at different temperatures. It is apparent that sintering does not start until 1000°C, at which temperature sintering has just started and there is a system of interconnected pores at the nanometer scale. At 1100°C the amount of sintering is increased and some areas are fully densified, but some retain the interconnected porosity as seen at 1000°C. The samples sintered at 1200°C are shown to be highly dense with discrete nanometer sized pores. At 1300°C, as in the 1200°C, the HA particles seem fully sintered, but discrete pores around micron in size start to appear.

Figure 7 contains the micrographs of the CoHA pellet cross-sections sintered at different temperatures. At 700°C, sintering has not begun in CoHA pellets, and the samples retain the interconnected micro porosity seen in the HA samples sintered at 900°C. At 800 and 900°C sintering has begun but the interconnected micro porosity is

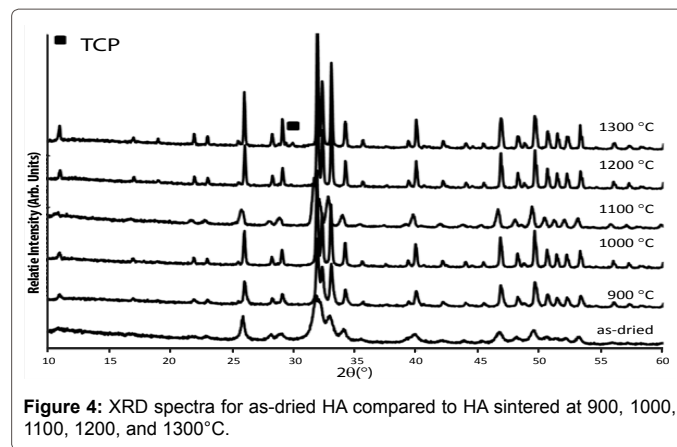


**Figure 4:** XRD spectra for as-dried HA compared to HA sintered at 900, 1000, 1100, 1200, and 1300°C.

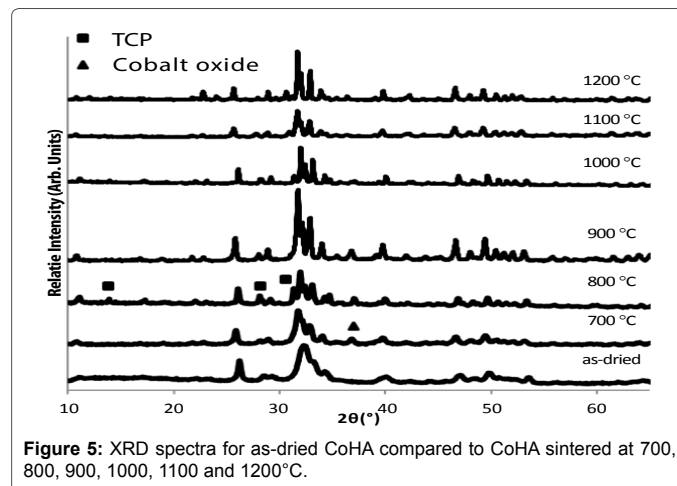


**Figure 5:** XRD spectra for as-dried CoHA compared to CoHA sintered at 700, 800, 900, 1000, 1100 and 1200°C.

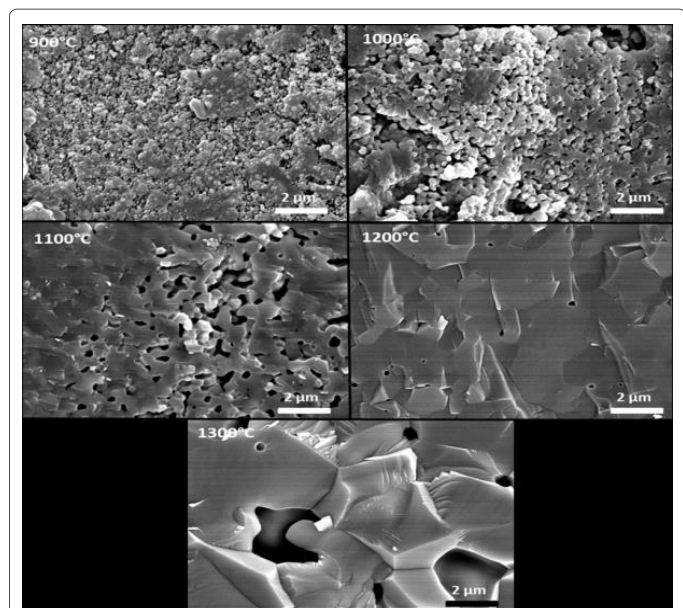


**Figure 6:** Cross sections of HA pellets sintered at 900, 1000, 1100, 1200 and 1300°C.

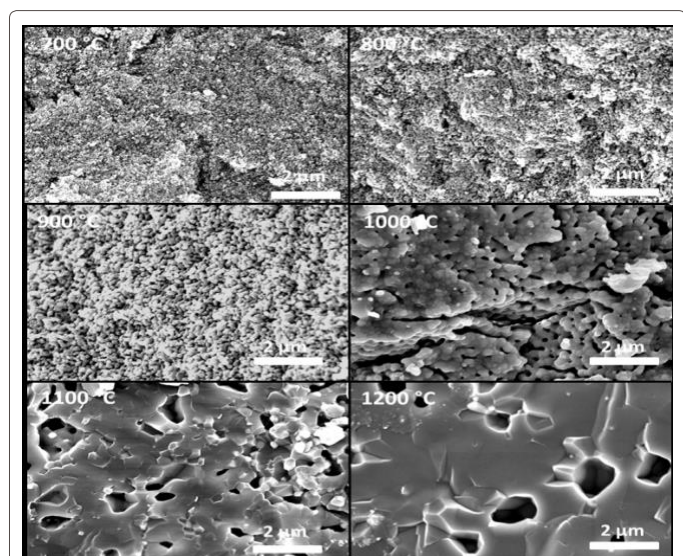


**Figure 7:** Cross sections of CoHA pellets sintered at 700, 800, 900, 1000, 1100 and 1200°C.

preserved, and the pellets still retain a morphology that is reflective of a packed powder. At 1000°C, sintering is well underway and the CoHA particles are no longer clearly differentiated. The pellets at 1000°C contain dense regions but are still highly porous with seemingly interconnected pores. The CoHA pellets sintered at 1100 and 1200°C are essentially a fully dense material interspersed with micron sized pores. The level of porosity is greater than that seen in the HA sintered at 1200 and 1300°C. Additionally, pore number decreases from 1100 to 1200°C, but pore size increases.

### Cell culture study

The effect of CoHA on cellular proliferation was inhibitive, while HA supported cell proliferation, as seen in Figure 8. The HA treated cells proliferated at the same rate over the course of one week. In

contrast the CoHA treated cells did not proliferate from day 1 to 3 with the optical density (O.D.) remaining the same while the cell number decreased from day 3 to 7 with a decrease in O.D.. The LDH assay results are presented in Figure 9. There is no statistical difference (as determined by a 2-tailed t-test) between the spontaneous release of LDH in cells treated with medium alone and those treated with HA or CoHA at 3 or 7 day time points.

### Discussion

HA can generally be sintered up to 1200°C or above before it is decomposed to TCP and CaO [26,27]. In this study, HA was sintered from 900°C up to 1300°C and cobalt substituted HA was sintered from 700°C up to 1200°C. The HA pellets underwent shrinkage (from an average diameter of 12.81 mm for the green pellets down to an average diameter of 10.17 mm for pellets sintered at 1200°C) but otherwise retained their white appearance with flat top and bottom surfaces. The CoHA pellets, on the other hand, underwent not only shrinkage but also an obvious color change upon sintering.

CoHA sintered pellets have obvious visual differences compared to the pure HA pellets, but densification behavior and mechanical properties show similar trends, although the actual densities and MOR achieved are different. HA pellet density increased until 1200°C, and at 1300°C began to drop. CoHA pellet density also increased to 1200°C,

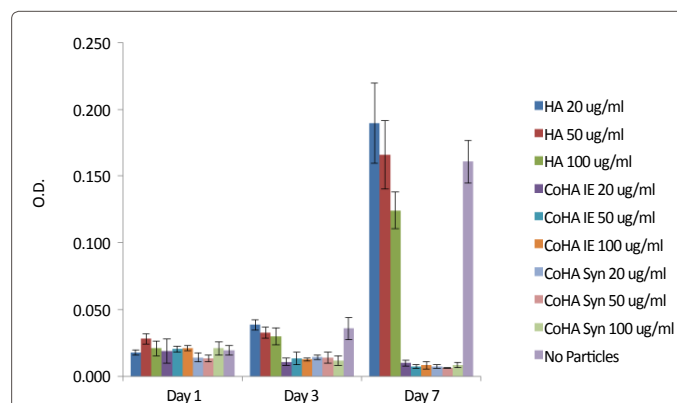


**Figure 8:** Cellular proliferation of cells treated with HA and CoHA supernatants in a 48 well plate. CoHA samples are identified as IE (generated via ion exchange procedure) or Syn (generated via wet synthesis).

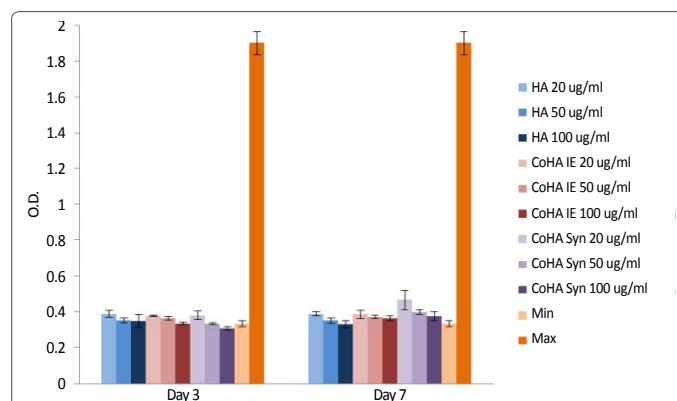


**Figure 9:** LDH release of cells incubated with supernatant from HA and CoHA for 24 hours. CoHA samples are identified as IE (generated via ion exchange procedure) or Syn (generated via wet synthesis). Min and Max samples refer to the control groups treated with normal cell culture medium and a lysis solution, respectively.

with the largest increase coming between 900 and 1000°C, but the actual densities achieved were lower than those achieved with pure HA at the same temperatures. For example, for pellets sintered at 900, 1000, and 1100°C, the density of HA samples are 2.50, 2.73, and 2.86 g/cm<sup>3</sup>, respectively, but CoHA pellets sintered at the same temperatures have average densities of 1.70, 2.15, and 2.45 g/cm<sup>3</sup>, respectively. This is unsurprising considering that the green density of CoHA was also lower than that of pure HA. The overall trend of increasing density is to be expected, since densification typically increases with sintering temperature prior to the onset of significant decomposition [28]. At their peak density, the HA pellets attain a density of 2.92 g/cm<sup>3</sup> sintered at 1200°C, which is 93% of the theoretical density of HA (3.156 g/cm<sup>3</sup>). The density of CoHA on the other hand, never approaches the theoretical density of HA within the temperature range tested. CoHA density in this study peaked at 2.46 g/cm<sup>3</sup>, which is only 78% the theoretical density of HA.

Considering the lower achieved densities, the MOR of the CoHA pellets are also lower than that of the HA pellets. The HA pellets achieve a maximum MOR value of 56.50 MPa, a value that compares favorably to the mechanical properties of bulk HA achieved by other groups in the literature [28,29], and is also within the mechanical properties range of natural bone, which possesses flexural modulus values ranging from 35 to 283 MPa [30]. CoHA achieved a maximum MOR value of 28.86 MPa, slightly below the low end of the range of flexural modulus values for natural bone.

The MOR is displayed as a function of sintering temperature in Figure 3. For pure HA, the MOR roughly plateaus between 1000 and 1100°C, with a slightly decrease at 1200°C. A significant decrease in MOR at 1300°C corresponds to a decrease in pellet density. This decrease may be due to the onset of decomposition of HA at high temperatures. The MOR of the CoHA pellets increase steadily to 1100°C and begins to decrease significantly at 1200°C, despite the fact that density has not yet begun to decrease at that temperature point.

The porosity of the sintered HA pellets dramatically increased at 1300°C, as shown by the FESEM images and corroborated by the decrease in density shown in Figure 2. The increase in both number and size of micropores at 1300°C compared to 1200°C may be due to increased decomposition. Sintering initially causes the close of pores, but concurrent dehydroxylation results in the formation of an internal vapor pressure that eventually overcomes the mechanical strength of the solid, resulting in the formation of blowholes. At higher temperatures a large amount of irreversible dehydroxylation occurs coupled with decomposition, of which water vapor is a product, leading to a collapse of the hydrated HA structure, and a large increase in blowhole area [31].

The CoHA pellets were shown to have increased porosity at 1200°C, as compared to 1100°C. This increase in porosity was accompanied by a decrease in MOR, despite a slight increase in overall density. At no sintering temperature are the density and porosity of the HA sintered at 1200°C approximated by the CoHA pellets. This is likely a result of an earlier onset of decomposition and formation of blowholes in CoHA than in HA. A similar result was also observed for iron-substituted HA, which decomposed at 700°C [32]. In addition to the density and mechanical property measurements, it is clear from visual inspection that the CoHA pellets have a different sintering behavior than the pure HA. It is likely caused by the presence of cobalt ions in the HA lattice resulting in a less stable crystal structure, thereby resulting in decomposition and formation of second phases at lower temperatures than those initiating decomposition in HA. XRD analysis

was conducted and confirmed this hypothesis.

A single-phase HA was achieved at sintering temperatures up to 1200°C, which was indicated by no extraneous peaks being present in the relative XRD spectra in Figure 4, which mimics typical sintering behavior in pure HA [26,27]. The emergence of an extraneous peak at 30° 2θ, which can be assigned to TCP, indicates the onset of decomposition. This explains the decrease in density and mechanical properties observed in the HA pellets sintered at 1200 and 1300°C. CoHA pellets were found to be less thermally stable than the HA, and emergence of a second phase started as low as 700°C, with emergence of TCP peaks indicating decomposition occurring as low as 800°C.

In CoHA sintered at 800°C and above extraneous peaks emerged at about 13.5, 28, and 31° 2θ. Each of these three peaks can be assigned to TCP, which has major peaks at 13.64, 27.79, and 31.05° 2θ. At 700°C and above there is also an obvious extraneous peak at about 36.5° 2θ. Neither HA nor TCP have XRD peaks at this location, so the possibility must be investigated that this peak belongs to an emerging cobalt containing phase, likely a cobalt oxide or hydroxide. Possibilities, determined by which cobalt oxide and hydroxide phases have significant peaks around 36.5° 2θ, include CoO, Co<sub>3</sub>O<sub>4</sub>, and Co(OH)<sub>3</sub>.

Unfortunately, other significant peaks for these materials overlap with HA and TCP peaks, so direct identification based on extraneous peaks is difficult, since sintered CoHA pellets likely contain varying mixtures of calcium phosphate (HA and TCP) and cobalt oxide and hydroxide phases. From 600-700°C, CoO is readily oxidized in air to Co<sub>3</sub>O<sub>4</sub>. This behavior, combined with the fact that Co<sub>3</sub>O<sub>4</sub> is characterized by a typical black color accounting for the color change seen in the CoHA pellet sintered at 700°C, allows us to conclude that Co<sub>3</sub>O<sub>4</sub> is present in the CoHA pellets sintered at 700°C. Examination of the calcium phosphate peaks in the XRD spectra for this sample indicates that at 700°C the Co<sub>3</sub>O<sub>4</sub> is present mostly in combination with HA. Beginning at 800°C we see a change in pellet color away from black and towards an increasingly muddy greyish brownish color. Our XRD results suggest that TCP also starts to emerge at this temperature. Samples sintered at 800°C and above are therefore combinations of HA, TCP, and changing cobalt oxide or hydroxide phases. Above 900°C CoO is thermally stable (as opposed to Co<sub>3</sub>O<sub>4</sub>), but can be readily oxidized to Co(OH)<sub>3</sub>. CoO has a characteristic olive color, whereas Co(OH)<sub>3</sub> is grayish brownish in color. From 800°C to 1200°C there is probably a phase change from Co<sub>3</sub>O<sub>4</sub> to Co(OH)<sub>3</sub>.

This conclusion is based on an inspection of the color change seen in the pellets combined with knowledge about cobalt oxide and hydroxide relative thermal stabilities, oxidation behaviors, and characteristic XRD spectra. In summary, we can conclude that CoHA samples sintered in air undergo various phase transformations from pure CoHA to apatite plus cobalt oxide, then further transform to a combination of calcium phosphate phases (mostly HA and TCP) plus a combination of cobalt oxide and hydroxide phases, with cobalt hydroxide dominating at higher temperatures.

The incorporation of cobalt ions into the HA lattice in the form of CoHA results in a material that is less thermally stable than pure HA, as proven by the difference in decomposition behavior as a result of sintering. Additionally, the relatively lower density and MOR of CoHA compared to HA make CoHA less suitable for bulk applications, particularly those which are load bearing, since a MOR within the range of natural bone was not achieved by the CoHA material. Even

bulk HA is typically used only in low-load-bearing situations, and the mechanical strength of CoHA is even more poor.

The CoHA material may, however, be useful in biomedical applications which call for nanoparticles in powder form, or as a coating or filler phase in a composite, specifically applications which utilize paramagnetic properties. The lower stability of the CoHA material compared to the HA control indicates that sintering of CoHA for bulk applications is not possible. Furthermore, since crystallinity, which affects ceramic solubility and biodegradation, is increased by sintering, a slower degradation rate could be achieved for a pure HA material than for CoHA [33]. The inability to sinter, combined with the calcium deficiency of the CoHA material compared to HA, suggests that a faster degradation *in vivo* is likely with CoHA [34]. A faster degradation rate may be a desirable trait for certain applications which call for short-term use of nanoparticles.

Prior to utilization in biomedical applications, the biocompatibility of CoHA needs to be evaluated. While the results from the proliferation experiment may initially suggest that CoHA is not biocompatible, the findings from the LDH assay, Figure 9, suggest differently. The discrepancy between these results suggests that either a catalytic reaction occurs between CoHA and the cell culture medium or the release of cobalt ions inhibits cell proliferation. The cell culture studies presented in this chapter are also limited in that a single cell line was used. Various cell lines may react differently to differing culture conditions. For example, Wu et al. established that low amounts of cobalt incorporation into a scaffold resulted in no cytotoxicity in human bone marrow stromal cells (BMSCs). Additionally, cobalt ion release from the scaffold induced VEGF protein secretion, HIF-1 $\alpha$  expression, and bone-related gene expression in BMSCs, indicating that while cobalt ions result in a response that mimics hypoxic conditions, they did not induce toxicity or cell death [35]. Additionally, *in vitro* cell culture conditions are simple and static, as compared to *in vivo* conditions. *In vivo* response to cobalt release from CoHA may differ from that seen *in vitro*. The cell culture results obtained in this chapter are not sufficient to draw any strong conclusions, and the CoHA material needs to be further investigated for its biocompatibility.

## Conclusion

The sintering behavior of CoHA, a magnetic biodegradable nanoparticle material, was thoroughly examined in this study. Density measurements, mechanical testing, FESEM, and XRD analysis were used to elucidate the sintering behavior of CoHA as compared to pure HA. It was found that CoHA has a lower stability than pure HA, and begins to decompose into a multi-phase material containing HA and cobalt oxide at temperatures as low as 700°C, and HA, TCP, and cobalt oxide and hydroxide at temperatures of 800°C and above. It is expected, based on these results, that CoHA will degrade more quickly *in vivo* than pure HA. Thus, together with other characterization of CoHA (magnetic properties and biocompatibility), it is suggested that CoHA is a biomaterial suitable for applications which require fast biodegradable magnetic materials in a powder form, such as drug delivery, MRI contrast agents, or hyperthermia cancer treatments. It can also be used as a coating on metallic substrates or as a filler for preparation of composites for different biomedical applications.

## Acknowledgement

The authors would like to thank the U.S. Department of Education Graduate Assistance in Areas of National Need (GAANN) Fellowship Program (P200A09315) and National Science Foundation (BES 0503315 and CBET-1133883) for their support of the research.

## References

1. Dee KC, Puleo DA, Bizios R (2002) An Introduction to Tissue-Biomaterial Interactions. Wiley-Liss, Hoboken, New Jersey.
2. Park JB, Bronzino JD (2003) Biomaterials Principles and Applications. CRC Press, Boca Raton, London New York, Washington, D.C.
3. Gibson IR, Ke S, Best SM, Bonfield W (2001) Effect of powder characteristics on the sinterability of hydroxyapatite powders. *J Mat Sci* 12: 163-171.
4. Martini FH (2003) Fundamentals of Anatomy & Physiology. Pearson- Benjamin Cummings, San Francisco.
5. Weiner S, Wagner HD (1998) The Material Bone: Structure-Mechanical Function Relations. *An Rev Mat Res* 28: 271-298.
6. Elliot JC (1994) Structure and Chemistry of the Apatites and Other Calcium Orthophosphates. Elsevier Science, Amsterdam.
7. Kay MI, Young RA (1964) Crystal Structure of Hydroxyapatite. *Nature* 204: 1050-1052.
8. Qu H, Vasiliev AV, Aindow M, Wei M (2005) Incorporation of Fluorine Ions in Hydroxyapatite by a pH Cycling Method. *J Mat Sci Mat Med* 16: 447-453.
9. Jiang M, Terra J, Rossi AM, Morales MA, BaggioSaitovitch EM, et al. (2002) Fe<sup>2+</sup>/Fe<sup>3+</sup> substitution in hydroxyapatite: Theory and experiment. *Phy Rev B, Condensed Matter and Materials Physics* 66.
10. Wang J, Nonami T, Yubata K (2008) Synthesis, structure and photophysical properties of iron containing hydroxyapatite prepared by a modified pseudo-body solution. *J Mat Sci Mat Med* 19: 2663-2667.
11. Wu HC, Wang TW, Sun JS, Wang WH (2007) A novel biomagnetic nanoparticle based on hydroxyapatite. *Nanotech* 18: 9
12. Morrissey R, Rodriguez-Lorenzo LM, Gross KA (2005) Influence of ferrous iron incorporation on the structure of hydroxyapatite. *J Mat Sci Mat Med* 16: 387-392.
13. Gross KA, Jackson R, Cashion JD, Rodriguez-Lorenzo LM (2002) Iron Substituted Apatites: A Resorbable Biomaterial with Potential Magnetic Properties. *Eur Cells Mat* 3: 114-117.
14. Prakash KH, Kumar R, Ooi CP, Sritharan T, Cheang P, et al. (2006) Wet Chemical Synthesis and Magnetic Property Studies of Fe(III) Ion Substituted Hydroxyapatite. *Molecular and Cell Biology* 3: 177-178.
15. Cazalhou S, Eichert D, Ranz X, Drouet C, Combes C, et al. (2005) Ion exchanges in apatites for biomedical applications. *J Mat Sci Mat Med* 16: 405-409.
16. Pankhurst QA, Connolly J, Jones SK, Dobson J (2003) Applications of magnetic nanoparticles in biomedicine. *J Phy D: Applies Physics* 36: R167-R181.
17. Duguet E, Vasseur S, Mornet S, Devoisselle JM. (2006) Magnetic nanoparticles and their applications in medicine. *Nanomedicine* 1: 157-168.
18. Jain TK, Richey J, Strand M, Leslie-Pelecky DL, Flask CA, et al. (2008) Magnetic nanoparticles with dual functional properties: Drug delivery and magnetic resonance imaging. *Biomaterials* 29: 4012-4021.
19. Lu AH, Salabas EL, Schüth F (2007) Magnetic Nanoparticles: Synthesis, Protection, Functionalization, and Application. *Angew Chem Int Ed*, 46: 1222-1244.
20. Gupta AK, Gupta M (2005) Synthesis and surface engineering of iron oxide nanoparticles for biomedical applications. *Biomaterials* 26: 3995-4021.
21. Markides H, Rotherham M, El Haj AJ (2012) Biocompatibility and Toxicity of Magnetic Nanoparticles in Regenerative Medicine. *J Nano Mat* 2012: 614094.
22. Stojanovic Z, Veselinovic L, Markovic S, Ignjatovic N, Uskokovic D (2009) Hydrothermal Synthesis of Nanosized Pure and Cobalt-Exchanged Hydroxyapatite. *Mat Manufac Process* 24: 1096-1103.
23. Veselinovic L, Karanovic L, Stojanovic Z, Bracko I, Markovic S, et al. (2010) Crystal structure of cobalt-substituted calcium hydroxyapatite nanopowders prepared by hydrothermal processing. *J App Crystallogr* 43: 320-327.
24. Kramer E, Itzkowitz E, Wei M (2014) Synthesis and Characterization of Cobalt-Substituted Hydroxyapatite Powders. *Ceramics International*: In press.
25. ASTM Standard F 394 (1996) "Test Method for Biaxial Flexure Strength (Modulus of Rupture) of Ceramic Substrates," ASTM International, West Conshohocken.
26. Ruys AJ, Sorrell CC, Brandwood A, Milthorpe BK (1995) Hydroxyapatite

- sintering characteristics: correlation with powder morphology by high resolution microscopy. *J Mat Sci Lett* 14: 744-747.
27. Finoli A, McKeef D, Gerlach J, Nettleship I (2010) Phase transformation behavior of hydroxyapatite foams subject to heat treatment. *Biomed Mat* 5:1
  28. Pattanayak DK, Divya P, Upadhyay S, Prasad RC, Bao BT, et al. (2005) Synthesis and Evaluation of Hydroxyapatite Ceramics. *Trends Biomater Artif Organs* 18: 87-92.
  29. Pattanayak DK, Dash R, Prasad RC, Rao BT, Rama Mahan TR (2007) Synthesis and sintered properties evaluation of calcium phosphate ceramics. *Materials Science and Engineering C: Materials for Biological Applications* 27: 654-690.
  30. An YH, Draughn RA (2005) *Mechanical Testing of Bone and Bone-Implant Interface*. CRC Press, Boca Raton.
  31. Ruys AJ, Wei M, Sorrell CC, Dickson MR, Brandwood A, et al. (1995) Sintering effects on the strength of hydroxyapatite. *Biomaterials* 16: 409-415.
  32. Kramer E, Wei M (2013) A comparative study of the sintering behavior of pure and iron-substituted hydroxyapatite. *BDA* 3: 9
  33. Yang Y, Dennison D, Ong JL (2005) Protein adsorption and osteoblast precursor cell attachment to hydroxyapatite of different crystallinities. *The Int J Oral & Maxillofacial Implants* 20: 187-192.
  34. Ginebra MP, Fernandez E, Driessens FCM, Pianell JA (1999) Modeling of the hydrolysis of  $\alpha$ -tricalcium phosphate. *J Am Cer Soc* 82: 2808-2812.
  35. Wu C, Zhou Y, Fan W, Han P, Chang J, et al. (2012) Hypoxia-mimicking mesoporous bioactive glass scaffolds with controllable cobalt ion release for bone tissue engineering. *Biomaterials* 33: 2076-2085.